Measurement 223 (2023) 113781

Contents lists available at ScienceDirect

Measurement

journal homepage: www.elsevier.com/locate/measurement

Real-time monitoring of ground-tire rubber microwave devulcanization with thermal and electrochemical sensors

Rafael Pérez-Campos, José Fayos-Fernández *, Juan Monzó-Cabrera

Departamento de Tecnologías de la Información y las Comunicaciones, Universidad Politécnica de Cartagena, 30202 Cartagena, Spain

ARTICLE INFO

Keywords:
Ground-tyre rubber
Microwave devulcanization
Sulphur gases
Dielectric properties
Electrochemical sensors

ABSTRACT

Devulcanizing ground-tire rubber (GTR) properly requires the removal of the sulphur linkages that crosslink the polymer. The volatile sulphur compounds (VSCs) released during the process must be extracted from the reactor to avoid any chemical recombination, and the sulphur gas concentrations conveniently sensed during the extraction, along with a thermal sensoring of the payload, can be used to monitor the whole devulcanization process. In this contribution, a modified conventional microwave oven was used to devulcanize the GTR. The microwave-processed GTR was evaluated by determining the values of its mass loss (ML), soluble fraction (sol fraction), and the variation of its electric permittivity. Results show a direct relationship between the energy delivered, sol fraction, the VSCs concentrations, the ML, and the permittivity values. Thus, this paper demonstrates that monitoring the VSCs can provide a reliable indication of ML and, consequently, devulcanization evolution even at non-uniform temperature conditions.

1. Introduction

The old practice of landfilling tires has been unable to keep up with the residue production of End-of-Life Tires (ELTs) due to their slow rate of decomposition. Additionally, the insufficient recovery flowrate of their materials and fire risks occurring at storage sites make the management of ELTs a global environmental challenge.

ELTs are mainly made of vulcanized rubber, which is chemically very stable and not readily biodegradable due to its crosslinked structure, stabilizers, and other additives. Therefore, efficient recycling methods are being proposed [1,2]. During the vulcanization process, the crosslinking of the rubber polymer main chains turns the thermoplastic into a thermoset material that cannot be remoulded applying just heat and mechanical forces. As a result, the cross-linked network of vulcanized rubber must be broken down via certain thermophysical, biological, or chemical processes [1,2] so that it can be processed again in a manner comparable to that of virgin rubber.

The value of ground tire rubber (GTR) as a rubber feedstock for the manufacturing industry is based on its ability to be processed to produce thermoplastic elastomers and blends in composite materials, and devulcanization has become the most appropriate method [3]. This process involves removing sulphur from the three-dimensional structure formed during vulcanization while preventing elastomeric chain damage. As a result, in order to ensure the high quality of the devulcanized GTR, sufficient energy must be applied to cleave the sulphidic bonds formed during vulcanization while preserving the carbon bonds [4].

Amid the several possibilities for devulcanizing rubber, microwave devulcanization has some advantages that make it one of the most promising techniques in rubber recycling [5,6]. These benefits include reducing processing time and energy, having the ability to treat large amounts of material in a continuous process, and the ease with which process parameters such as power level and treatment time can be adjusted. This is critical since each rubber compound has particular characteristics and a chemical composition that requires a specific level of devulcanization in order to produce a usable substance [7].

However, some molecular interactions of the rubber with the electromagnetic field are required for the microwave energy to heat and break the crosslinks. This can be accomplished in non-polar elastomers by using conductive fillers such as carbon black, which is typically used as a reinforcing filler in rubber compositions used for GTR [8]. In this way, microwave energy can be absorbed and turned into heat within the GTR matrix, i.e., the GTR temperature increases as a consequence of the microwave treatment.

The final temperature of GTR was formerly thought to be the main factor in determining whether the devulcanization procedure was

* Corresponding author.
E-mail addresses: rafael.perez@upct.es (R. Pérez-Campos), jose.fayos@upct.es (J. Fayos-Fernández), juan.monzo@upct.es (J. Monzó-Cabrera).

https://doi.org/10.1016/j.measurement.2023.113781
Received 27 July 2023; Received in revised form 11 October 2023; Accepted 26 October 2023
Available online 29 October 2023

successful. Thus, the parameter most frequently employed to regulate the microwave process is rubber temperature. In some studies, the temperature was monitored during the whole microwave process [9–13]. However, other researchers opted to record the rubber temperature only after the microwave treatment [7,14–19]. In other contributions [20–24], their authors evaluated the processed rubber, but the temperature was not monitored in real time.

Nonetheless, some previous works indicate that it is difficult to build an adequate temperature monitoring and control subsystem on a laboratory scale [6,9], thereby requiring a methodology to evaluate the process during microwave treatment [6]. One option might be to utilize the microwave energy transmitted to the cavity as a parameter to assess the process [10,19,21]. Nevertheless, many variables influence heating performance (e.g., the irradiated electric field distribution, the evolution of both the absorbed power and the electromagnetic properties of the material through the process), making it difficult to adequately assess the process by controlling only the energy transmitted. This fact emphasize the importance of using other methods to evaluate the microwave devulcanization process in real-time.

According to several recent studies, the gaseous by-products of devulcanization could be used as control and monitoring variables [25,26]. Song et al. [17], for instance, came to the conclusion that the desulphurization reaction and the sulphur generated during the microwave procedure are related, and according to [25], some major chains are broken during the microwave processing of waste rubber, releasing volatile organic compounds (VOCs) and VSCs, including hydrogen sulphide (H_2S), sulphur dioxide (SO_2), and carbon disulphide (CS_2). However, to the best knowledge of the authors, there is not any contribution that uses the monitoring of the sulphur gases released during the microwave irradiation of GTR and relates it to the most important devulcanization variables and yields.

In this work, sulphur gas concentrations and temperature levels were monitored while GTR was irradiated with various microwave power regimes and underwent a devulcanization process. The measurements of sulphur gas concentrations have been related to several important process parameters, such as the mass loss, the irradiated power levels, the GTR absorbed energy, its temperature evolution, the changes observed in the Fourier Transform Infrared (FTIR) analysis, those observed in the scanning electron microscope (SEM), the results from the Soxhlet extraction, and the changes in the GTR complex's relative electric permittivity, to better understand the microwave processing of GTR and to provide the basis for the improvement and innovation of this process.

Despite the fact that permittivity is seldom employed to evaluate the processed rubber, in this contribution, it was evaluated by measuring its permittivity since it is directly related to its chemical composition and structure, as explained in our previous work [27]. Permittivity controls a material's reactivity to electromagnetic fields. The permittivity of empty space ($\varepsilon_0 = 8.854{\cdot}10^{-12}$ F/m) is used to normalize the absolute permittivity and to obtain the so-called relative permittivity (ε_r). It is a complex variable that is commonly expressed by the equation (1):

$$\varepsilon_r = \varepsilon_r{}' - j{\cdot}\varepsilon_r{}'' \tag{1}$$

where $\varepsilon_r{}'$ and $\varepsilon_r{}''$ stand for the loss factor and dielectric constant, respectively, and are referred to as the dielectric properties. The quantity of electric energy that may be stored inside the irradiated material depends on the real component of permittivity (the dielectric constant), whereas the imaginary part (the loss factor) represents the material's capacity to transform microwave radiation into heat. Thus, the ratio between the loss factor and the dielectric constant defines the material's ability to be heated under the influence of a microwave field and is called its loss tangent ($\tan\delta = \frac{\varepsilon_r{}''}{\varepsilon_r{}'}$).

2. Materials and methods

The material under test (MUT) was crumb rubber from ELTs (GTR), kindly provided by Synthelast (Spain). The GTR had an apparent bulk density of 400 kg/m^3, with granule sizes ranging from 0.5 to 1 mm. The MUT's primary components are as follows [27]: natural rubber (36 %), carbon black (27 %), synthetic rubber (22 %), inorganic components (8.5 %), additives and oil (4.6 %), and sulphur (1.9 %).

2.1. MUT mass loss determination

It was used 300 ± 0.1 g of GTR to prepare the batches inside a quartz dish (Duran, reference 213135906, Germany). This initial mass decreased during an effective microwave processing when gaseous by-products are generated; hence, the MUT batch was weighed before and after the microwave devulcanization process using a scale with a 0.1 g precision (GRAM, series SV, Spain). Every test's mass loss percentage was calculated using equation (2):

$$ML(\%) = \left(1 - \frac{M_a}{M_i}\right){\cdot}100 \tag{2}$$

where M_a corresponds to the MUT mass after being processed and M_i is the initial MUT mass (300 g).

2.2. Sulphur gas concentration monitoring

Among the several types of gas sensors on the market, electrochemical gas sensors are one of the inexpensive gas sensors that are most frequently used to check air quality. These sensors have the ability to track the levels of several VOCs, VSCs, and other gases. Additionally, they provide a short response and a broad sensitivity range from mg/m^3 to g/m^3 [28]. Samad et al. [29] investigated the electrochemical gas sensor response under various conditions and concluded that it could provide a great opportunity to collect high-quality data on air pollutants. Additionally, in [26], three electrochemical sensors were employed to track the VSCs generated during the microwave-assisted devulcanization of GTR in the presence of nitrogen and a small oxygen percentage. When these VSCs were generated during the microwave irradiation, the experimental trials in this study demonstrated that the pyrometer was severely blinded.

The following is a detailed explanation of how this type of sensor works: when a target gas molecule encounters the sensor, it first passes through an anti-condensation membrane, which acts as a dust shield. Subsequently, gas molecules get diffused through a capillary filter, and afterwards, they must cross a hydrophobic membrane to reach the surface of the sensing electrode. At this point, the molecules are immediately oxidized or reduced as a consequence of reacting with analytes, producing or consuming electrons as a result. Thus, sensors can generate an electrical current signal proportional to the gas concentration.

In this contribution, one of each type of electrochemical sensor among the H2S/CG-2000, SO2/CF-2000, and CS2/PF-500 models from Membrapor (Switzerland) was used to monitor the concentration of H_2S, SO_2, and CS_2 during the process. One of the primary justifications for using various sulphur gas sensors instead of a single one is the possibility that certain gases released during the process may have a detrimental effect on sulphur gas detection. Hence, employing various sulphur gas sensors reduces the likelihood of errors caused by interfering gases. The sensors were connected to a motherboard containing a microcontroller and an EEPROM memory for storing sensor-specific data, such as calibration parameters. The resolution of each type of sulphur gas sensor is 1, 0.5, and 0.5 parts per million (ppm) for sensing H_2S, SO_2, and CS_2, respectively.

2.3. MUT dielectric properties characterization

The dielectric properties of the MUT were measured using a Dielectric Kit for Vials (DKV) from the ITACA research institute of the Universidad Politècnica de Valencia (Spain). In order to determine the

reflection coefficient at each frequency, this apparatus sends a microwave frequency-swept stimulus into a resonant cavity and measures the power consequently reflected. Since this equipment is based on a perturbational method (relative measurements), the calibration has to be performed while its cavity is empty as the standard reference and before loading the cavity with the sample to be measured. The resonance frequency shift of the response signal with and without the material and the resonance bandwidth expansion due to a decrease in cavity quality factor (losses caused by the loaded material) are used to quantify the dielectric constant and loss factor of the MUT at around 2.45 GHz. The relative complex permittivity is obtained from the variation of the resonance response using numerical methods based on mode-matching and circuit analysis techniques, as discussed in [30].

The DKV's operating frequencies range from 1.5 to 2.6 GHz, and it can characterize materials with dielectric constants less than 100 and loss factors between 0.001 and 15. This device has an accuracy of 1 % and up to 5 % for the dielectric constant and loss factor, respectively. The manufacturer rates the repeatability and linearity at 0.2 %.

Three samples of 2 g were prepared per processed batch of 300 g of GTR after it cooled down to room temperature, leading to volumes of 5 cm^3. Quasi-cylindrical polypropylene test tubes (Deltalab, reference 400,400, Spain) were used as sample containers. An in-house analog volumeter with parallax error control and a resolution of 0.1 cm^3 was used to determine the sample volume, as employed in [31]. A permittivity test was run for each batch, and the average of every set of three samples per batch was considered for the analysis.

2.4. FTIR analysis

The chemical structure of the samples was examined through FTIR analysis conducted with a Nicolet 5700 spectrometer (Thermo Scientific, Madison, USA). Spectral data was recorded with a resolution of 4 cm^{-1} and 32 scans were taken in the range of 500–4000 cm^{-1}.

2.5. Soxhlet extraction

To ascertain the impact of microwave treatment on GTR, the sol fraction of the microwave-processed sample was analyzed through

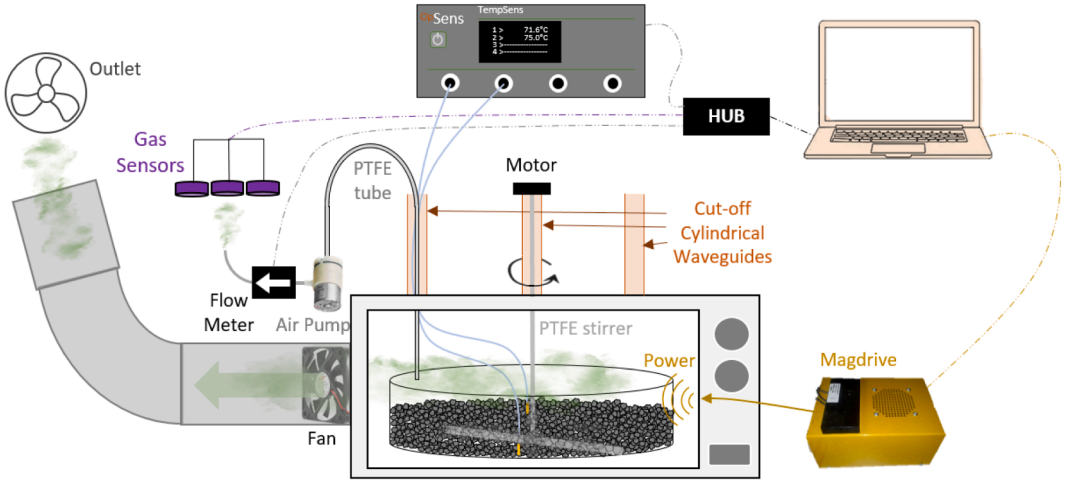

(a)

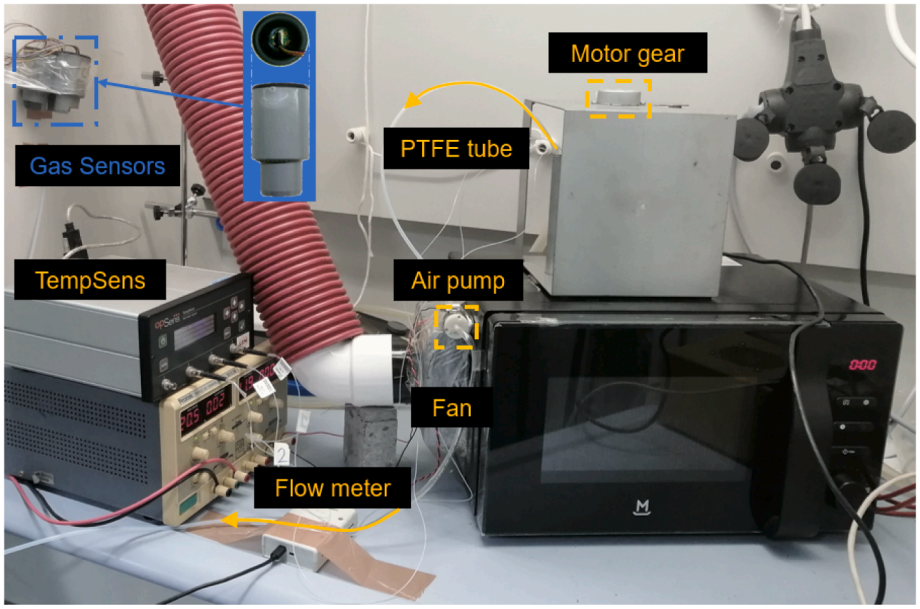

(b)

Fig. 1. Experimental system. (a) Schematic diagram. (b) Actual setup.

Soxhlet extraction, employing toluene as the solvent. The extraction length was 24 h, utilizing approximately 5 g of material. After the extraction, both the material and the thimble filter were dried for 24 h at 80 °C, and the sample mass was measured.

2.6. Microwave-assisted devulcanization setup

Despite the fact that commercial microwave oven are readily available in the market, for this research, a modified conventional microwave oven offering very similar advantages and limitations has been employed, as elaborated upon below.

Three metallic tubes were welded to the microwave cavity upper wall, with their 1.6 cm hollow diameter serving as by-passes for the connection of accessories and sensors inside the cavity, as shown in Fig. 1. The length of 14.5 cm of such tubes ensured a cut-off cylindrical waveguide configuration, acting as microwave filters that avoided radiation leakage outwards, as long as no metallic wiring or rods were inserted through the tubes.

Aiming for homogeneous processing of the payload as a bulk, that is, achieving the most uniform time-averaged temperature pattern possible for the MUT, a motorized polytetrafluoroethylene (PTFE) stirrer was employed. The stirrer shaft, which transmits torque from the external motor to the stirrer blades inserted into the MUT with a rotational speed of 5 rpm, was passed through the central by-pass tube, as shown in Fig. 1. The stirring speed is set at 5 rpm to align with the capability of the motor, which corresponds to that integrated in the microwave for plate rotation.

Through a drilled area (with hole diameters of 2.5 mm) at the left side wall, the mainstream of gaseous devulcanizing by-products were forcibly pulled out of the cavity using an axial fan (Nidec Beta SL, D07R-12T2S4, Japan) with a maximum flowrate of 33.6 m^3/hour, ensuring appropriate ventilation of the cavity. In light of the significant consequences associated with the recombination of sulphur in its gaseous form, which can detrimentally affect the processing ability of devulcanized rubber [32], it is imperative to prevent such recombination. In addition to that, the role of the fan in preventing prolonged gas retention within the cavity is emphasized, thereby averting the development of exceedingly high sulphur gas concentrations that might saturate the gas sensors. The fan intake was attached to the exterior of the drilled cavity wall, effectively reducing its flowrate rating. The fan exhaust was gathered by a flexible tube and directed toward a fume hood, which kept the gases under control and enabled a secure working environment.

The use of pyrometers or infrared cameras for monitoring the GTR surface temperature from a zenithal point is not reliable during the effective process of devulcanization, as described in [26], since fumes produced during chemical reactions blind both types of sensors. Therefore, two optical fiber sensors (OpSens, OTG-A, Canada) connected to a signal conditioner (OpSens, TempSens, Canada) were used to estimate the MUT's temperature. According to the manufacturer's specifications, the measurement accuracy for temperatures below 45 °C is 0.3 °C and 0.8 °C for temperatures above 45 °C.

The sensor tips were placed in diametrically opposite positions on the inner walls of the quartz container, in contact with the GTR granules, as depicted in Fig. 2. This configuration avoided having uncontrolled floating measurement points and the risk of damaging the sensors due to twisting of the optical fibers. A lower temperature for the GTR than the actual one was obtained because the quartz would lower the temperatures of the rubber and sensors at those locations.

The concentration levels of H_2S, SO_2, and CS_2 were monitored by the electrochemical sensors with the support of a subsystem that continuously sampled the atmosphere within the cavity. The intake of a PTFE hose was placed over the GTR surface, situated on the side nearest to the fan. This configuration ensures the gases generated during the tests are directed towards the PTFE intake, facilitating their direct access to the gas sensors. The airflow was forced towards the gas sensors by an air pump, as shown in Fig. 1(a). The airflow rate was registered by an FS2012 flowmeter (Renesas, Japan).

2.7. Irradiated power regimes

The microwave power was generated by a 2.45 GHz, 1 kW power-rated magnetron, fed by a controllable switched-mode power supply (Dipolar AB, MagDrive 1000, Sweden). For all tests, constant microwave power was supplied by the magnetron. As a consequence of the chemical structure modifications in GTR, which were clearly visible as VSCs were emanated, the dielectric properties of GTR increased [27]. This fact leads to faster heating, and hence pulsed on–off cycles were used to avoid thermal runaway, as explained in [33]. The microwave treatment parameters, such as the power level transmitted to the cavity, the number of pulses, the energy versus mass ratio (relative energy), as well as the nomenclature of the tests, are described in Table 1.

Fig. 3 shows the power profiles for each test. In certain tests, the power was reactivated only after the gases were evacuated from the cavity. Each test ended with the MUT being allowed to cool down without any microwave power being applied.

For the 230 W power level profile, a single pulse was applied. Three tests under this profile were performed, applying different irradiation periods. For the 460 W power level profile, two tests were performed with three on–off cycles, and two additional tests had six on–off cycles. Regarding the 690 W power level profile, two tests were performed with one on–off cycle, and two additional tests had two on–off cycles.

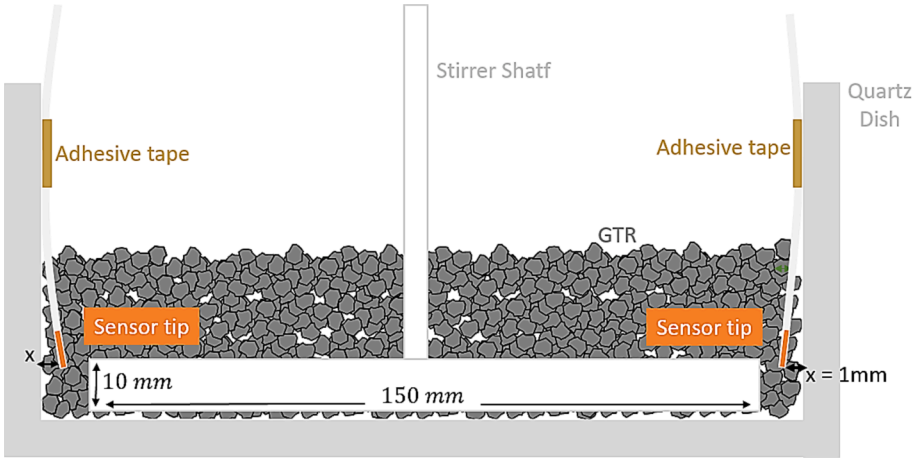

Fig. 2. Schematic diagram of the fiber optic sensors positioning.

Table 1
Parameters of microwave processing and test abbreviations.

Abbreviation	Power (W)	Number of power pulses	Relative energy to process the MUT (J/g)
230 W 1p 571 J/g	230	1	571
230 W 1p 765 J/g	230	1	765
230 W 1p 939 J/g	230	1	939
460 W 3p 803 J/g	460	3	803
460 W 3p 1152 J/g	460	3	1152
460 W 6p 1025 J/g	460	6	1025
460 W 6p 1089 J/g	460	6	1089
690 W 1p 826 J/g	690	1	826
690 W 1p 1052 J/g	690	1	1052
690 W 2p 808 J/g	690	2	808
690 W 2p 856 J/g	690	2	856

2.8. MUT surface temperature distribution

The effectiveness of the stirring mechanism, whose purpose was to ease homogeneous processing, was estimated by acquiring thermal images of the MUT surface at the end of some testing processes with some specific continuous wave irradiation profiles: 230 W during 11 min, 460 W during 7 min, and 690 W during 6 min. The different timing for each profile responds to the strategy of heating the payload as much as possible without causing the production of fumes that would have distorted the thermal imaging. The thermographs were registered using an infrared camera (Fluke, Ti25, U.S.A.), whose thermal images have 160 × 120 pixels with a spatial resolution of 2.5 mrad/pixel (in both elevation and azimuth). This means that the recorded termographs had a spatial resolution of 1.7 mm since the measurement distance from the GTR surface was 70 cm. The accuracy of the instrument is 2 °C or 2 % for its temperature measurement range of −20 °C to 350 °C. The emissivity parameter was set to 0.9.

The protocol for this thermal imaging required a withdrawal of the batch out of the cavity as soon as the microwave power had been switched off. To avoid damage risks to the fiber optic sensors attached to the pyrex container and to perform the measurements as fast as possible, none of these fibers were used in these tests. It is assumed that the delay between the irradiation stop and the thermal snapshot did not significantly distorted the temperature distribution due to the low thermal conductivity of GTR, which is around 0.017 W/m·K [34], and the high radiation emissivity, between 0.8 and 0.96 [35].

2.9. Energy transmitted by the magnetron

The amount of energy delivered by the magnetron (W_{del}) to the cavity has been determined as a function of the time-discretised power transmitted (P_{del}) for an irradiation time as described in equation (3):

$$W_{del} = \sum_{k=1}^{N} \frac{P_{del}(t_k) + P_{del}(t_{k-1})}{2} \cdot (t_k - t_{k-1});\ N \geq 1 \quad (3)$$

where t_k and $P_{del}(t_k)$ are the elapsed time and power records for the *k-th* sample, respectively. In this study, the time sampling resolution $(t_k - t_{k-1})$ was set to 1 s. The irradiation started at $t_0 = 0s$.

Most of this delivered energy will be absorbed by the MUT, but a residual loss is expected to be dissipated in both the magnetron due to power reflections and other elements within the cavity (e.g., cavity walls, pyrex recipient).

2.10. Estimation of absorbed energy from temperature measurements

Devices such as directional couplers or reflectometers could have been employed to measure the incident and reflected power at the cavity feeding port to determine the power supplied to the GTR batch. However, in this work, the sensible temperature of GTR has been used to estimate the microwave energy absorbed by the MUT by using the measurements of the optical fiber sensors, as described in [27]. Therefore, the time-discretized sensible absorbed power (P_{abs}) parameter is defined in Eq. (4):

$$P_{abs}(t_k) = m_{GTR} \cdot C_p \cdot \frac{\Delta T_k}{\Delta t_k} = m_{GTR} \cdot C_p \cdot \frac{T_k - T_{k-1}}{t_k - t_{k-1}};\ k \geq 1 \quad (4)$$

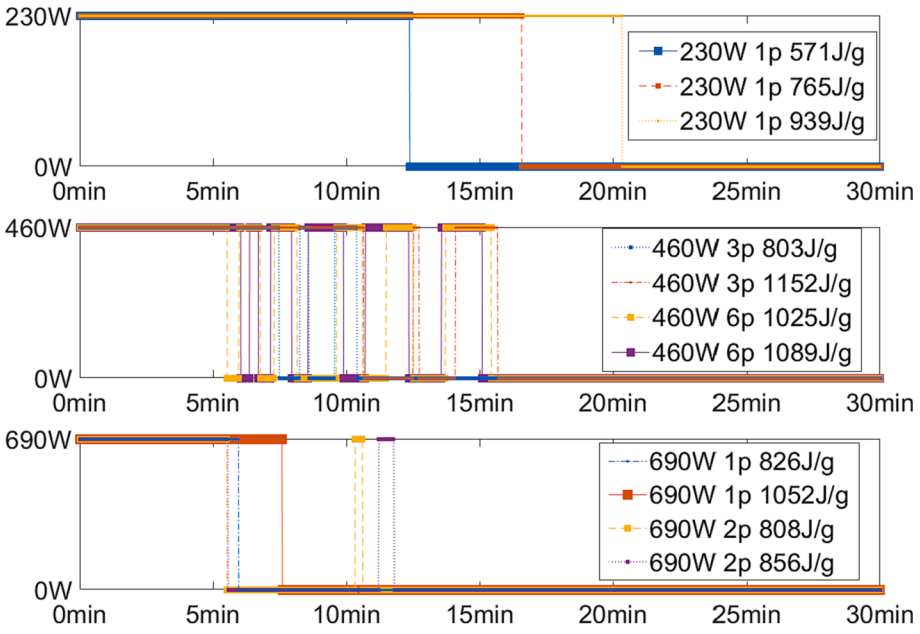

Fig. 3. Power profiles transmitted by the magnetron.

where m_{GTR} (g) is the initial GTR bacth mass, $C_p(J{\cdot}g^{-1}{\cdot}K^{-1})$ is the GTR specific heat, and ΔT_k (°C) is the temperature variation for the time interval Δt_k (s). For all calculations, the specific heat value for GTR batches was assumed to be 1.9 $J{\cdot}g^{-1}{\cdot}K^{-1}$ [36], even though this parameter is expected to vary dynamically with temperature and with the level of effectiveness of the processing throughout the batch [37].

Using this sensible absorbed power, P_{abs}, the amount of sensible energy absorbed (W_{abs}) by the MUT can be computed as

$$W_{abs} = \sum_{k=1}^{N} P_{abs}(t_k)\cdot(t_k - t_{k-1});\ N \geq 1 \quad (5)$$

2.11. Concentration of sulphur gases released during the microwave treatment

The sulphur gases released (*SG*) at any time has been determined considering a linear combination of all three measured concentrations of H_2S, SO_2, and CS_2, that is:

$$SG(t_k) = GC_{H2S}(t_k) + GC_{SO2}(t_k) + GC_{CS2}(t_k) \quad (6)$$

where GC_{H2S}, GC_{SO2}, and GC_{CS2} are the H_2S, SO_2 and CS_2 gas concentrations, in ppm, at the sampling time t_k, respectively.

Consequently, an estimation of the observed total amount of sulphur gases during the process was computed as the integral of the cumulative sulphur gas concentration throughout time as follows:

$$SG = \sum_{k=1}^{N} \frac{SG(t_{k-1}) + SG(t_k)}{2}(t_k - t_{k-1});\ N \geq 1 \quad (7)$$

2.12. Morphology

The Zeiss Crossbeam 350 field emission scanning electron microscope (FESEM) (Carl Zeiss Microscopy GmbH, Germany) was employed to examine the surface morphology of the GTR samples. The specific observation parameters were set as follows: an acceleration voltage of 2 kV and a working distance of 5 mm. The resulting image was created utilizing the secondary electron signal (SE Secondary Electron), and the data acquisition was carried out utilizing SmartSEM 6.07 software (Zeiss, Germany).

3. Results and discussion

3.1. Average temperature curves versus time

Fig. 4 shows the average temperature evolution for different power levels and irradiation configurations, as detailed in Table 1. Despite the fact that the power was constant in three groups of tests (230, 460, and 690 W), different initial average MUT heating rates were obtained for a fixed power level. This indicates that, even when using a dielectric PTFE stirrer, the temperature distribution was not completely homogeneous and that cold and hot spots affected the temperature measurement points differently for different tests. Other studies [6,9] support this conclusion by mentioning the difficulties in maintaining a uniform temperature distribution. Furthermore, because of the stirring process, it is possible that during some tests, the optical fiber (OF) sensors were closer to the holder wall and thus measured the holder-MUT effective temperature, whereas during others, the OF sensors were completely immersed in the MUT and thus measured higher temperatures.

For the test 230 W 1p 939 J/g with the longest irradiation time in Fig. 4a, a higher final temperature is observed, as expected, although a thermal runaway effect could be operating if we compare this temperature rise to 460 W tests with higher energy levels. In the 460-W tests, after the gases appeared, a sequence of power pulses was introduced, resulting in similar temperature patterns. Additionally, no significant temperature growth was observed during these tests, and this seems to indicate that power-off cycles could be beneficial in batch temperature redistribution, thereby avoiding the thermal runaway effect. Different results can be seen in the 690 W tests, where large temperature increases are most likely due to the thermal runaway effect.

3.2. Evolution of the sulphur gas concentration increments over time

Fig. 5 depicts the increments of the sulphur gas concentrations versus time for all tests. To accurately visualize the sulphur gas concentration gradients, only the first power pulse was used to calculate them. Sulphur gas concentration gradients were nearly zero before the gases emerged, as expected, indicating that there is a threshold condition for devulcanization as deduced from [27]. The analysis is interesting once the gases appear because the concentration gradients grow abruptly until a

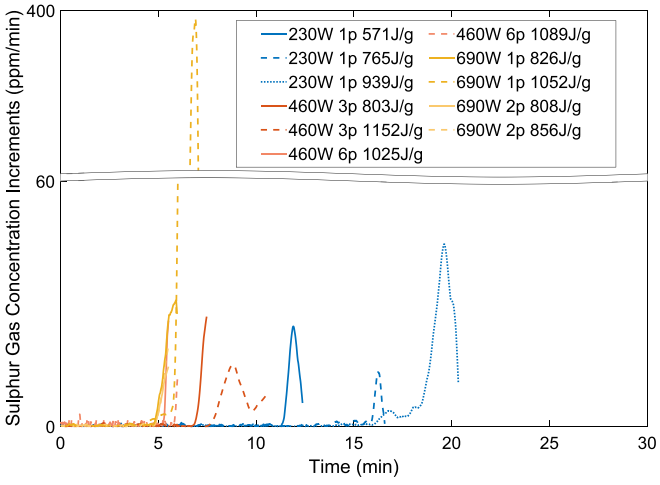

Fig. 5. Sulphur gas concentration gradients versus time.

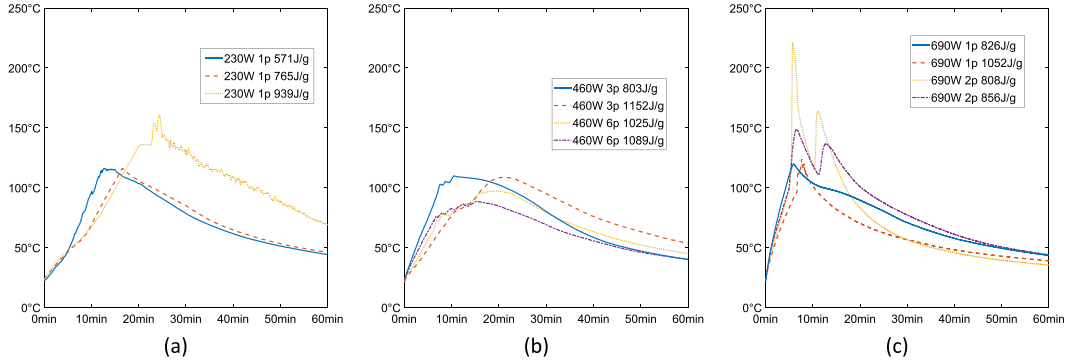

Fig. 4. Temperature profiles versus time for different power levels and on/off cycles. (a) 230 W. (b) 460 W. (c) 690 W.

certain maximum is reached. This implies that the majority of the weaker (in terms of energy) sulphidic bonds have been broken. The gradient will ascend again if the power pulse is long enough, as observed in the 460 W 3p 1152 J/g test. The tests in which higher power and energy levels were employed (e.g., 690 W 1p 1052 J/g) are those in which the gases appear in first place, perhaps due to runaway processes located at hot spots. As a matter of fact, the tests with higher levels of delivered energy but more uniform temperature behaviour, such as 460 W 6p 1025 J/g or 460 W 6p 1089 J/g promote gas liberation at much lower concentration levels.

3.3. Sulphur gas concentration behaviours versus temperature

Fig. 6 plots the sulphur gas concentrations versus the average GTR temperature, considering only the first power pulse so as to make the data as clear as possible. The majority of tests show that sulphur gases appear when the average temperature recorded by the fiber optic (FO) sensors reaches 110 °C. Other experiments, such as the 460 W 3p 803 J/g or 460 W 3p 1152 J/g tests, revealed that gases were present at considerably lower temperatures, implying that the GTR batch's other parts were at higher temperatures and that the stirrer was unable to evenly distribute their temperature.

In fact, a prior study conducted under monomode settings and with significantly more uniform heating patterns [27] found that chemical changes commence at temperatures ranging between 150 and 195 °C. The MUT temperature readings for each test, however, demonstrate a general tendency in which temperature values are lower than anticipated when sulphur gases are initially identified. The OF sensors were placed close to the holder wall to prevent the stirrer from moving and breaking them. Therefore, instead of monitoring the MUT temperature, OF sensors may be measuring the temperature of the quartz dish or the MUT-holder effective temperature, which is one potential explanation supported by the results in the following section. Similar threshold temperature values were observed by other authors who employed a conventional microwave oven [38].

3.4. GTR temperature distribution

The thermographs obtained at 230, 460, and 690 W are shown in Fig. 7. As can be seen, a significant proportion of the MUT offers similar temperature values to those given by the FOs when the sulphur gases arise, i.e., 110 °C, especially at the container's surface.

Fig. 7 allows us to draw three important conclusions:

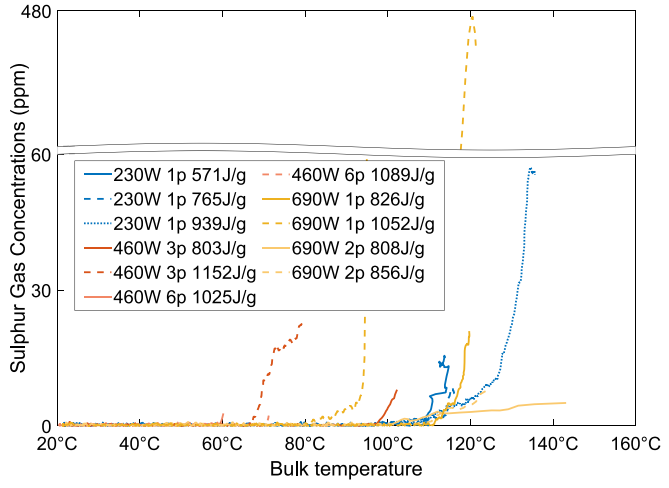

Fig. 6. Sulphur gas concentration evolution versus average temperature for different irradiated power and energy levels.

- Despite the use of stirring processes and regardless of power level, hot spots can be detected in all thermographs.
- Due to thermal losses at the container-air interface, the temperature is always much lower than the temperature in the container's central regions.
- Finally, the thermographs show that the more power used, the higher the average temperature of the GTR.

These findings explain why the temperature at which the gases appear varies so greatly between tests, as well as why these temperatures are lower than those reported in [27]. The position of the FO becomes critical due to the batch's heterogeneous temperature distribution.

From the results shown in Fig. 7, therefore, it can be concluded that it is very difficult to monitor the microwave devulcanization of GTR in multimode applicators by using temperature sensors due to the non-uniformity of heating patterns, even when stirring is utilized, and the generation of gases that blind no-contact sensors like pyrometers or thermal cameras. An alternative approach to addressing this issue of temperature distribution in the sample is to employ a monomode cavity. Nonetheless, this results in a significantly reduced sample size for each test, thus posing challenges for evaluating the sample e.g., by means of its dielectric properties.

3.5. Sulphur gas concentration evolutions versus microwave energy consumed

Fig. 8 depicts the evolution of sulphur gas concentrations in relation to the relative energy (J/g) delivered by the magnetron. When calculating this energy, Eq. (3) was taken into account. The results show that the presence of sulphur gases requires a minimum relative delivered energy of about 500 J/g. However, the energy required for other tests varies greatly, with some requiring more than 700 J/g delivered in order for the MUT to release gases. There are several reasons for this:

- Inefficient GTR stirring results in non-homogeneous temperature distributions where microwave energy is concentrated in hot spots, resulting in higher energy density distributions in hot spots and the earlier appearance of gases.
- Various levels of power reflection may occur during the tests, resulting in varying amounts of absorbed microwave power in the GTR.

In Fig. 8, it can also be observed the appearance of sulphur gas concentration peaks and valleys that can be associated with power on–off cycles, although with some inertia since gases continue to appear even after energy transmission has been interrupted. This is due to the time needed for the sulphur gases to escape from the GTR matrix and the time they need to arrive at the sensors due to the air flux.

The difference in threshold energy shown in Fig. 8 might be explained by the differences in hot-spot distribution for each test. The onset of sulphur gases implies that GTR is undergoing some chemical changes and, as a result, the value of its dielectric properties increases, as stated in [27]. Thus, if the power transmission continues, thermal runaway may occur. Hence, more microwave energy is converted into thermal energy, causing the temperature of the hot spots to rapidly rise. Accordingly, despite the fact that the measured batch average temperature is lower than expected, sulphur gases appear at these hot spots.

3.6. Sulphur gas concentration behaviours over energy absorbed by the GTR

Fig. 9 depicts the evolution of sulphur gas concentrations in relation to the batch's relative energy (J/g). This energy was calculated using Eqs. (4) and (5). To improve visualization, only the first power pulse was used to determine the absorbed energy. According to the results, the

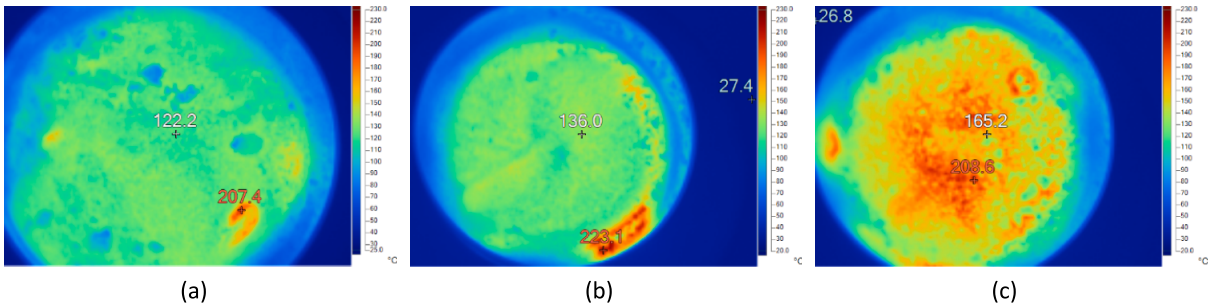

Fig. 7. Thermographs after tests using different constant power levels. (a) 230 W. (b) 460 W. (c) 690 W.

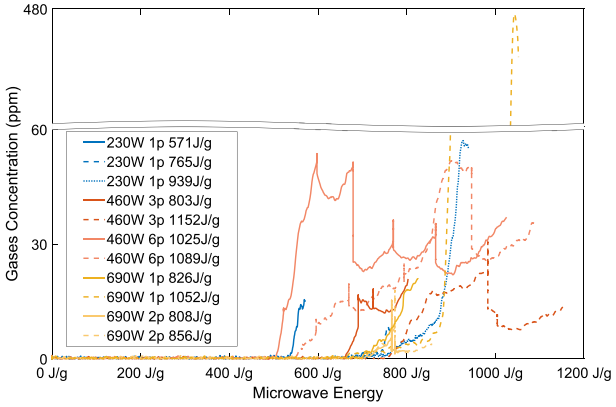

Fig. 8. Sulphur gas concentrations versus energy transmitted by the magnetron.

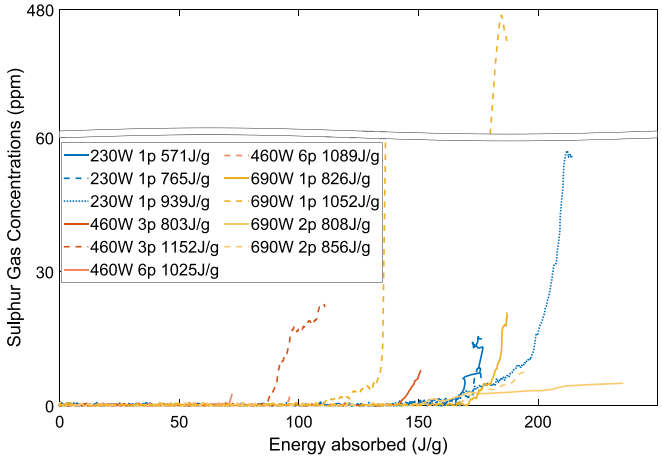

Fig. 9. Sulphur gas concentration evolutions versus sensible absorbed energy.

presence of sulphur gases necessitates a minimum relative absorbed energy of about 70 J/g. The energy required for other tests, on the other hand, varies greatly, with some requiring more than 150 J/g absorbed for the MUT to release gases.

These relative energy thresholds are lower than the relative energy threshold levels shown in [27], where relative energies for permittivity changes range between 240 and 320 J/g. The thermal losses and resulting lower temperatures at the container surface where the optical fiber sensors are located are the main reasons for this. As a direct consequence, Eqs. (4) and (5) show that the absorbed energy is underestimated in this work compared to [27], where uniform heating patterns were obtained.

The measured dispersion of absorbed energy threshold levels in this work is mainly due to the non-homogeneous temperature distributions given the inefficient GTR stirring, which leads to situations where microwave energy is concentrated in hot spots, resulting in higher energy density distributions in some areas.

3.7. Characterization by FTIR

The FTIR results are depicted in Fig. 10. A certain noise is noticeable in the 2000–2300 cm^{-1} and 3300–4000 cm^{-1} ranges. Consequently, data smoothing was applied to enhance its visual quality. The peaks associated with the C–H bonds located within the 3000–2800 cm^{-1} range do not exhibit differences between the original GTR and the devulcanized GTR samples. This suggests that the hydrocarbon backbone of the GTR was not degraded by microwave processing.

A distinct peak at approximately 1730 cm^{-1} corresponds to the C=O bond, confirming the presence of carbon black in the GTR. It is noteworthy that this peak is consistently present in all samples, that is, in the original GTR and in the microwave-processed samples. The region of the FTIR spectrum related to the carbonyl around 1540 cm^{-1} reveals that significant changes took place during the microwave treatments. In fact, the peaks corresponding to C=C bonds disappear in the spectra of some devulcanized GTR samples.

The CH_2 bands (around 1450 cm^{-1}) refer to the vibrations of stretching and aromatic bending of the SBR, and the CH_3 bands (1390–1372 cm^{-1}) are indicative of natural rubber groups. These bands were consistently observed in all the FTIR analyses, suggesting that the GTR did not undergo significant degradation because of the microwave processing. Hence, the results suggest that the main macromolecular structure of the rubber was partially affected by the microwave devulcanization process, i.e., C–H bonds remained unaffected, but some C=C bonds were broken, as observed in [14].

Furthermore, it is evident that the bands corresponding to CH_2 deformation (1440 cm^{-1}), CH_3 asymmetric deformation (1375 cm^{-1}),

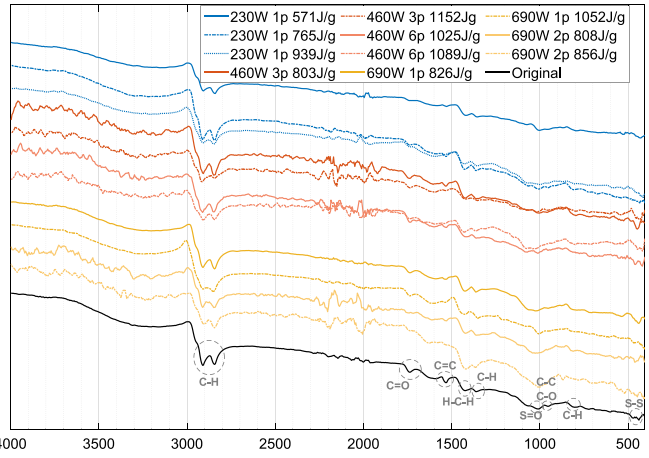

Fig. 10. FTIR spectra for the GTR samples.

S=O (1050 cm^{-1}), C–C (980 cm^{-1}), C–O (980 cm^{-1}), and =CH out-of-plane bending (820 cm^{-1}) underwent certain modifications due to the microwave treatment. The single band at around 1050 cm^{-1} can be attributed to sulfonyl groups, and it is present in all GTR samples. These findings confirm that an oxidative degradation of the main polymer chain occurred simultaneously with the rubber devulcanization during the microwave treatment, as explained in [21].

Additionally, in the FTIR spectra within the 500–400 cm^{-1} range, there is a reduction in the peak heights associated with S–S bonds for the microwave-processed GTR samples. This fact confirms the breaking of a significant proportion of the vulcanization bonds. To enhance the FTIR results, further studies are envisaged with an improved setup that ensures better temperature uniformity and a more homogeneous material.

3.8. Mass loss (ML) dependency on sulphur gas concentration evolutions

The GTR under test is heated during the microwave processing, which causes the release of several types of gases and a consequent reduction in mass. The MUT temperature and the ML have a direct connection; the higher the temperature, the higher the ML. As stated in [39], the volatilization of the processing oil and other low-boiling-point components causes around 9 % of the overall mass to be lost at temperatures below 300 °C. At these temperatures, certain sulphidic bonds are also broken, releasing sulphur gases. However, as explained in previous sections, monitoring the MUT temperature during devulcanization is a complicated task. Therefore, in this section, the relationship of the ML to the total amount of detected sulphur gas concentrations is studied, as indicated in Eqs. (2), (6) and (7).

Fig. 11 depicts the ML percentage as a function of the total number of accumulated sulphur gas concentrations. Except for the 690 W 1p 1052 J/g test, where significantly high sulphur gas concentration values were found despite the ML not being among the highest, an obvious trend can be seen versus released sulphur gas for these temperature, power, and energy level ranges. A hot zone where microwave energy is focused and high levels of sulphur gas concentrations are emitted could be one reason for this exception.

This is supported by the observation that, despite having the highest relative energy and power level of the 690 W series, the recorded average temperature of the 690 W 1p 1052 J/g is the lowest, as the temperature sensors are unable to measure that hot spot. This implies that the remaining portion of the GTR batch is at a lower temperature, resulting in a lower ML percentage.

A linear function was used to fit the experimental data on *ML* dependence versus released sulphur gas. The data from the 690 W 1p 1052 J/g test was not considered for the data fitting. Equation (8) describes the mass loss behaviour over released sulphur gases data fittings:

$$\mathrm{ML(SG)} = 3.5{\cdot}10^{-4}{\cdot}\mathrm{SG} \tag{8}$$

where *SG* is the total sulphur gas concentration integrated during each test and calculated as indicated in Eqs. (6) and (7). The root mean square error (RMSE) and the coefficient of determination (R^2) for the mass loss are 0.785 and 0.922, respectively.

3.9. GTR dielectric properties evolution versus ML

Fig. 12 represents the relationship between mass loss percentage and loss tangent (tanδ). Greater values are observed for the loss tangent as *ML* increases, indicating that changes in the chemical composition of the MUT, which causes the release of VOCs and VSCs, are responsible for permittivity changes. Minor variations in the MUT's bulk density when measuring its dielectric properties, as well as non-uniform temperature profiles experienced during microwave processing in the MUT, from which the permittivity samples are collected, may explain the observed dispersion in the loss tangent values.

A linear function was used to fit the experimental data for the loss tangent dependence on ML. The loss tangent dependence on *ML* data fitting is described by Eq. (9):

$$\tan\delta\,(\mathrm{ML}) = 0.0028{\cdot}\mathrm{ML} + 0.016 \tag{9}$$

where *ML* is the mass loss in percentage (%). The RMSE and the R^2 values for the loss tangent are 0.002 and 0.948, respectively.

3.10. Sol content versus energy transmitted to the cavity

Fig. 13 shows the soluble contents of the GTR samples in relation to the relative microwave energy transmitted to the cavity. A general pattern can be observed, that is, the higher the microwave energy transmitted to the cavity, the higher the sol fraction, confirming the occurrence of devulcanization.

Taking solely the test employing a single power pulse into consideration, one can observe that the lower the power, the higher the sol content for comparable energy levels transmitted to the cavity. It seems that more pronounced temperature gradients within the sample are formed when higher power levels are used. Consequently, some parts of the sample are extensively processed, while others remain relatively unprocessed. Hence, the soluble content is lower, primarily because a larger portion of the sample has not undergone substantial processing.

An exponential function was used to model the relationship between the soluble content and the delivered microwave energy (MW_{energy}) at each power level, as described by Eq. (10):

$$\text{Soluble Content}\left(\mathrm{MW_{energy}}\right) = X_p{\cdot}e^{3.6{\cdot}MW_{energy}} + 9.25 \tag{10}$$

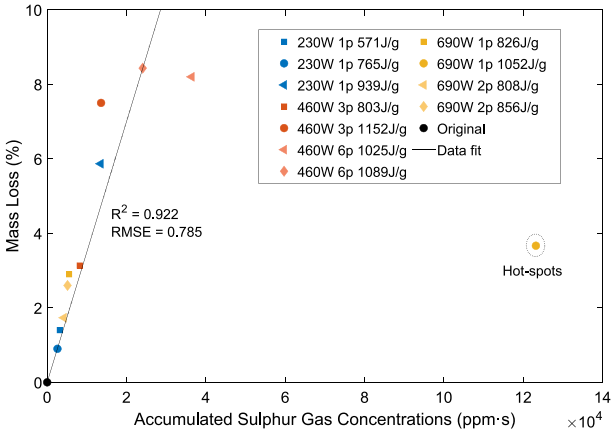

Fig. 11. ML evolution versus accumulated sulphur gas concentrations for different tests.

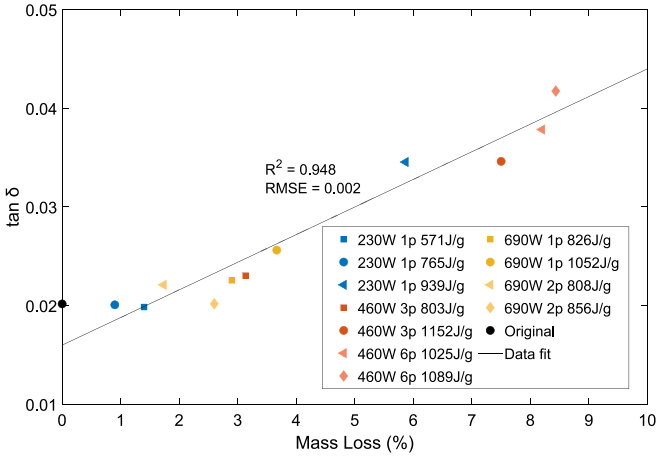

Fig. 12. Loss tangent evolution versus ML.

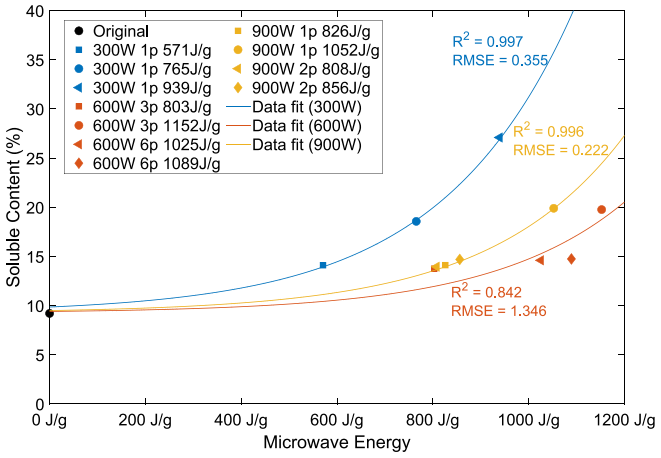

Fig. 13. Soluble content as a function of the microwave energy density transmitted to the cavity.

where MW_{energy} represents the microwave energy supplied by the magnetron (in kJ/g), and X_p is a constant value that varies depending on the data fitting. Specifically, its values are 0.6, 0.15, and 0.24 for the data fittings associated with tests using power levels of 230 W, 460 W, and 690 W. The RMSE for the data fittings at these respective power levels is 0.355, 1.346, and 0.222. As for the R^2, it is 0.997, 0.842, and is 0.996 for the tests employing 230 W, 460 W, and 690 W, respectively.

3.11. Dielectric properties as a function of microwave energy transmitted by the magnetron

The development of the dielectric properties in relation to the relative microwave energy provided by the magnetron is shown in Fig. 14. Despite the scattered data, a general pattern seems to exist: once a certain energy value is reached (i.e., a particular energy threshold seems to exists), permittivity rises with rising delivered energy, following an exponential pattern. The threshold energy for the loss factor, i.e., the minimal energy provided for permittivity to begin to change its initial value, appears to be around 800 J/g. However, this threshold energy is lower for the dielectric constant, at around 600 J/g.

Despite delivering a similar amount of energy, it is interesting to note that permittivity values for tests in which different power pulses were used (the "460 W 6p 1025 J/g" and "460 W 6p 1089 J/g" tests) are typically higher than those for tests in which only one pulse was used (the "690 W 1p 1052 J/g" test). One hypothesis is that when many power pulses are applied, the fact that microwave power is not delivered for a while helps to prevent sulphur that was ejected in gas form from returning to the MUT, thereby creating new sulphidic bonds. Another argument is that, compared to non-uniform temperature distributions, where the areas with lower temperature values produce lower dielectric and loss factor values, pulsing the microwave power allows for more uniform temperature profiles and improved heat redistribution. Thus, it seems evident that unequal temperature distributions would result in poorer permittivity data.

Two second-order polynomial functions were used to fit the experimental data for the permittivity dependence on delivered microwave energy (MW_{energy}). Both the dielectric constant and the loss factor data fittings are described by Eqs. (11) and (12):

$$\varepsilon_r^{'}\left(\mathrm{MW_{energy}}\right) = 0.5{\cdot}\mathrm{MW_{energy}}^2 - 0.1{\cdot}\mathrm{MW_{energy}} + 2.22 \tag{11}$$

$$\varepsilon_r^{''}\left(\mathrm{MW_{energy}}\right) = 0.1{\cdot}\mathrm{MW_{energy}}^2 - 0.06{\cdot}\mathrm{MW_{energy}} + 0.041 \tag{12}$$

where MW_{energy} is the microwave energy delivered by the magnetron (in kJ/g). The RMSE and the R^2 for the dielectric constant are 0.084 and 0.749, respectively. For the loss factor, the RMSE is 0.012 and the R^2 is 0.731.

3.12. SEM analysis

The SEM results are presented in Fig. 15. As can be seen, the original GTR particles exhibit a relatively smooth surface with minimal irregularities in their shape. In contrast, the devulcanized GTR particles corresponding to the 230 W 1p 571 J/g and 230 W 1p 765 J/g tests show small cracks, possibly attributable to mechanical stress changes. In the case of the remaining tests, in addition to the cracks, there are noticeable gullies and pores, likely resulting from the volumetric expansion of gas generated within the particles or the appearance of microplasmas. For most tests, the previously mentioned temperature variations in the sample are observed, whereby some particles show little modification while others exhibit multiple hollows due to the microwave treatment. As a general trend, it seems that the smaller particles are considerably more influenced by microwaves compared to their larger counterparts. This fact may be the primary explanation for the higher devulcanization percentages observed in smaller particle sizes, as demonstrated in [40].

4. Conclusions

In this study, the microwave processing of GTR in a multimode oven was monitored by measuring both the MUT temperature with FO sensors and the sulphur gas concentrations generated during the devulcanization process with the aid of electrochemical sensors. Several delivered power levels, on/off regimes, and energy values were employed while the GTR was agitated with a PTFE stirrer to obtain a better understanding of the GTR's microwave processing under these conditions. In addition, the internal structure changes of each microwave-processed MUT were assessed by measuring its dielectric properties and its *ML* percentage.

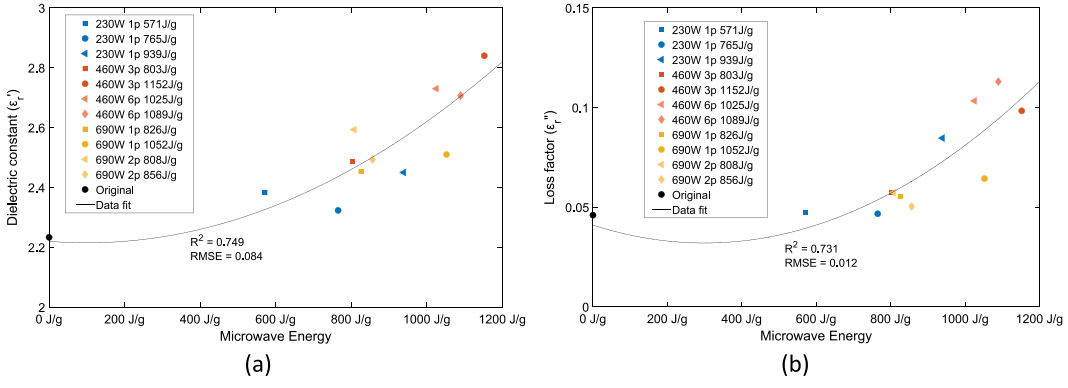

Fig. 14. Dielectric properties dependency on the microwave energy density (J/g) delivered to the applicator. (a) Dielectric constant. (b) Loss factor.

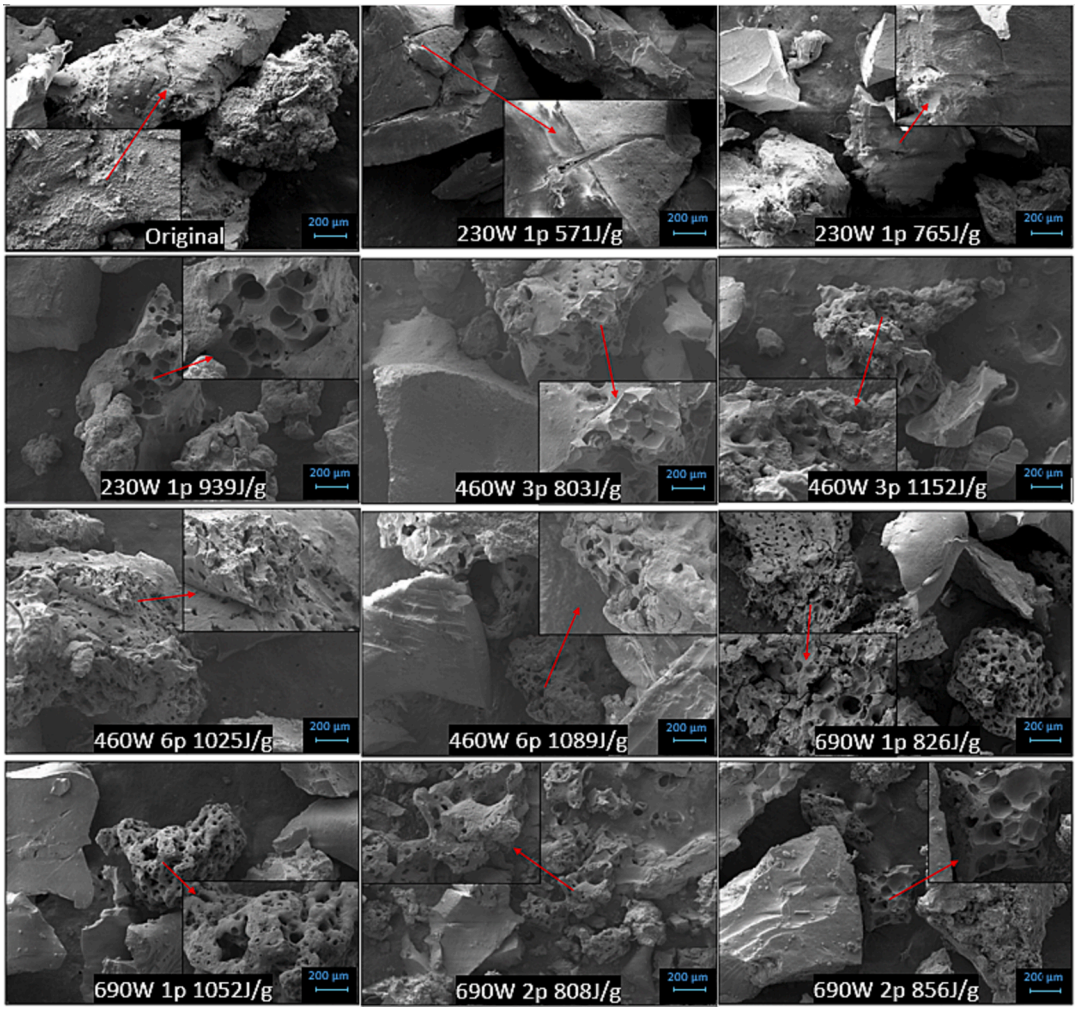

Fig. 15. SEM photographs of the original GTR sample and microwave-processed GTR samples.

Regarding the temperature records, some difficulties were found in adequately monitoring the MUT temperature. This is evident from the temperature profiles shown in Fig. 4, where different average temperature slopes are observed even when using the same power levels. In addition, the recorded thermal images revealed that some hot spots are generated during the microwave process. This indicates that properly monitoring microwave devulcanization of GTR with temperature sensors is a very complicated task unless optimal stirring is achieved for the GTR particles. This also points out the necessity of very efficient stirring mechanisms to achieve uniform devulcanization processes for high-volume batches.

Different energy thresholds in terms of released sulphur gases were observed. The energy thresholds seem to be mainly related to the stirrer efficiency. A heterogeneous temperature distribution is obtained when the stirring effectiveness is poor and, as a consequence, cold and hot spots appear. Thus, some parts of the batch reach the temperature threshold to emit gases, while other parts are still far from that.

A similar problem applies for the sensible absorbed energy. The minimum required absorbed energy for sulphur gases to form was, for most tests, around 170 J/g. This energy threshold is much lower than that found in [27], which ranged from 240 to 320 J/g. This fact may be explained by the capacity of the stirrer to provide uniform temperature patterns; if the batch temperature distribution is not uniform, several cold and hot spots are generated. As a result, sulphur gases are observed despite the fact that the average MUT temperature, and therefore the sensible absorbed energy, is much lower than the threshold one.

In this contribution, evident trends were observed between the *ML* and the dielectric properties, which are directly related to the GTR chemical composition and structure [27]. Taking into consideration that *ML* is due to the release of VOCs and VSCs, as well as the fact that *ML* has a direct connection with the average MUT temperature, *ML* can be considered a parameter to evaluate the MUT devulcanization. In this contribution, a relationship between the ML and the released sulphur gases was presented, implying that sulphur gases may become significantly useful in controlling the microwave processing of GTR.

The variations in permittivity values revealed that the chemical structure changed as a result of the microwave treatment. For tests with similar amounts of energy delivered by the magnetron, higher permittivity values were found for those in which several power pulses were applied compared to one-pulse tests. It seems that the fact that microwave power is not delivered between power pulses appears to be beneficial in preventing sulphur released in gaseous form from returning to the MUT. Furthermore, pulsing the microwave power results in a more homogeneous temperature distribution.

Because different GTR processing levels were discovered for similar amounts of employed energy, the results presented in this paper may aid in the optimization of GTR microwave devulcanization processes. Furthermore, there appears to be a strong correlation between sulphur gas concentrations, dielectric properties, and ML, implying that microwave processing of GTR could be evaluated in real-time by monitoring the VSCs released during the process. More research is planned to determine the precise relationship between permittivity changes, sulphur gas concentration evolution, and the types of sulphidic bonds broken (and formed) during the process, as well as the cure

characteristics and hardness of the microwave-assissted devulcanized GTR. With this objective in mind, specific modifications to the setup configuration are to be made to achieve an optimal experimental setup.

Funding

This research did not receive any specific grant from funding agencies in the public, commercial, or not-for-profit sectors.

Ethical approval

This article does not contain any studies with human participants or animals performed by any of the authors.

CRediT authorship contribution statement

Rafael Pérez-Campos: Conceptualization, Data curation, Formal analysis, Investigation, Methodology, Software, Validation, Visualization, Writing – original draft. **José Fayos-Fernández:** Formal analysis, Methodology, Resources, Supervision, Visualization, Writing – review & editing. **Juan Monzó-Cabrera:** Conceptualization, Methodology, Resources, Validation, Visualization, Writing – review & editing.

Declaration of Competing Interest

The authors declare that they have no known competing financial interests or personal relationships that could have appeared to influence the work reported in this paper.

Data availability

Data will be made available on request.

References

[1] K. Formela, Sustainable development of waste tires recycling technologies–recent advances, challenges and future trends, Adv. Ind. Eng. Pol. Res. 4 (3) (2021) 209–222, https://doi.org/10.1016/j.aiepr.2021.06.004.
[2] E. Markl, M. Lackner, Devulcanization technologies for recycling of tire-derived rubber: a review, Materials 13 (5) (2020), https://doi.org/10.3390/ma13051246.
[3] L. Asaro, M. Gratton, S. Seghar, N.A. Hocine, Recycling of rubber wastes by devulcanization, Resour. Conserv. Recycl. 133 (2018) 250–262, https://doi.org/10.1016/j.resconrec.2018.02.016.
[4] S. Ramarad, M. Khalid, C.T. Ratnam, A.L. Chuah, W. Rashmi, Waste tire rubber in polymer blends: a review on the evolution, properties and future, Prog. Mater Sci. 72 (2015) 100–140, https://doi.org/10.1016/j.pmatsci.2015.02.004.
[5] B. Adhikari, D. De, S. Maiti, Reclamation and recycling of waste rubber, Prog. Poly. Sci. 25 (7) (2000) 909–948, https://doi.org/10.1016/S0079-6700(00)00020-4.
[6] K. Formela, A. Hejna, L. Zedler, X. Colom Fajula, F.J. Cañavate Ávila, Microwave treatment in waste rubber recycling–recent advances and limitations, Exp. Polym. Lett. 13 (6) (2019) 565–588. https://www.doi.org/10.3144/expresspolymlett.2019.48.
[7] C. Scuracchio, D. Waki, M.L.C.P. Da Silva, Thermal analysis of ground tire rubber devulcanized by microwaves, J. Therm. Anal. Calorim. 87 (3) (2007) 893–897, https://doi.org/10.1007/s10973-005-7419-8.
[8] E.T. Thostenson, T.W. Chou, Microwave processing: fundamentals and applications, Compos. A: Appl. Sci. Manuf. 30 (9) (1999) 1055–1071, https://doi.org/10.1016/S1359-835X(99)00020-2.
[9] A. Bani, G. Polacco, G. Gallone, Microwave-induced devulcanization for poly (ethylene–propylene–diene) recycling, J. Appl. Polym. Sci. 120 (5) (2011) 2904–2911, https://doi.org/10.1002/app.33359.
[10] S. Seghar, N.A. Hocine, V. Mittal, S. Azem, F. Al-Zohbi, B. Schmaltz, N. Poirot, Devulcanization of styrene butadiene rubber by microwave energy: effect of the presence of ionic liquid, Exp. Polym. Lett. 9 (12) (2015). https://www.doi.org/10.3144/expresspolymlett.2015.97.
[11] D.A. Simon, I.Z. Halász, J. Karger-Kocsis, T. Bárány, Microwave devulcanized crumb rubbers in polypropylene based thermoplastic dynamic vulcanizates, Poly. J. 10 (7) (2018) 767, https://doi.org/10.3390/polym10070767.
[12] D.A. Simon, D.Z. Pirityi, T. Bárány, Devulcanization of ground tire rubber: microwave and thermomechanical approaches, Sci. Rep. 10 (1) (2020) 1–13, https://doi.org/10.1038/s41598-020-73543-w.
[13] D.A. Simon, D. Pirityi, P. Tamás-Bényei, T. Bárány, Microwave devulcanization of ground tire rubber and applicability in SBR compounds, J. Appl. Polym. Sci. 137 (6) (2020) 48351, https://doi.org/10.1002/app.48351.
[14] F.D. de Sousa, C.H. Scuracchio, G.H. Hu, S. Hoppe, Devulcanization of waste tire rubber by microwaves, Polym. Degrad. Stab. 138 (2017) 169–181, https://doi.org/10.1016/j.polymdegradstab.2017.03.008.
[15] D. Hirayama, C. Saron, Chemical modifications in styrene–butadiene rubber after microwave devulcanization, Ind. Eng. Chem. Res. 51 (10) (2012) 3975–3980, https://doi.org/10.1021/ie202077g.
[16] V. Pistor, C.H. Scuracchio, P.J. Oliveira, R. Fiorio, A.J. Zattera, Devulcanization of ethylene-propylene-diene polymer residues by microwave—influence of the presence of paraffinic oil, Polym. Eng. Sci. 51 (4) (2011) 697–703, https://doi.org/10.1002/pen.21875.
[17] Z. Song, Y. Yang, J. Sun, X. Zhao, W. Wang, Y. Mao, C. Ma, Effect of power level on the microwave pyrolysis of tire powder, Energy 127 (2017) 571–580, https://doi.org/10.1016/j.energy.2017.03.150.
[18] A. Zanchet, L.N. Carli, M. Giovanela, J.S. Crespo, C.H. Scuracchio, R.C. Nunes, Characterization of microwave-devulcanized composites of ground SBR scraps, J. Elastomers Plast. 41 (6) (2009) 497–507, https://doi.org/10.1177/0095244309345411.
[19] Ł. Zedler, M. Klein, M.R. Saeb, X. Colom, J. Cañavate, K. Formela, Synergistic effects of bitumen plasticization and microwave treatment on short-term devulcanization of ground tire rubber, Poly. J. 10 (11) (2018) 1265, https://doi.org/10.3390/polym10111265.
[20] X. Colom, A. Faliq, K. Formela, J. Cañavate, FTIR spectroscopic and thermogravimetric characterization of ground tyre rubber devulcanized by microwave treatment, Polym. Test. 52 (2016) 200–208, https://doi.org/10.1016/j.polymertesting.2016.04.020.
[21] K. Aoudia, S. Azem, N.A. Hocine, M. Gratton, V. Pettarin, S. Seghar, Recycling of waste tire rubber: microwave devulcanization and incorporation in a thermoset resin, J. Waste Manag. 60 (2017) 471–481, https://doi.org/10.1016/j.wasman.2016.10.051.
[22] P.S. Garcia, F.D.B. De Sousa, J.A. De Lima, S.A. Cruz, C.H. Scuracchio, Devulcanization of ground tire rubber: physical and chemical changes after different microwave exposure times, Exp. Polym. Lett. 9 (11) (2015). https://www.doi.org/10.3144/expresspolymlett.2015.91.
[23] X. Colom, M. Marín-Genescà, R. Mujal, K. Formela, J. Cañavate, Structural and physico-mechanical properties of natural rubber/GTR composites devulcanized by microwaves: influence of GTR source and irradiation time, J. Compos. Mater. 52 (22) (2018) 3099–3108, https://doi.org/10.1177/0021998318761554.
[24] S. Poyraz, Z. Liu, Y. Liu, X. Zhang, Devulcanization of scrap ground tire rubber and successive carbon nanotube growth by microwave irradiation, Curr. Org. Chem. 17 (20) (2013) 2243–2248. https://www.doi.org/10.2174/13852728113179990049.
[25] M. Gągol, G. Boczkaj, J. Haponiuk, K. Formela, Investigation of volatile low molecular weight compounds formed during continuous reclaiming of ground tire rubber, Polym. Degrad. Stab. 119 (2015) 113–120, https://doi.org/10.1016/j.polymdegradstab.2015.05.007.
[26] R. Pérez-Campos, J. Fayos-Fernández, J. Monzó-Cabrera, A. Díaz-Morcillo, A. Martínez-González, A. Lozano-Guerrero, Improved control on the microwave devulcanizing of ground tire rubber by means of sulphur gas sensors, in: 18th International Conference on Microwave and High-Frequency Applications (AMPERE 2021), 2021, pp. 146–153. <https://www.doi.org/10.5281/zenodo.5378213>.
[27] R. Pérez-Campos, J. Fayos-Fernández, J. Monzó-Cabrera, F. Martín Salamanca, J. López Valentín, J.M. Catalá-Civera, P. Plaza-González, J.R. Sánchez-Marín, Dynamic permittivity measurement of ground-tire rubber (GTR) during microwave-assisted Devulcanization, Poly. J. 14 (17) (2022) 3543, https://doi.org/10.3390/polym14173543.
[28] M. Gerboles, L. Spinelle, A. Borowiak, Brochure Low-Cost Sensors. Thoughts on the Quality of Data Measured by Sensors, European Commission: Ispra, Italy, 2017. <https://publications.jrc.ec.europa.eu/repository/bitstream/JRC107461/low_cost_sensors_web.pdf> (Accessed: 13-October-2022).
[29] A. Samad, D.R. Obando Nuñez, G.C. Solis Castillo, B. Laquai, U. Vogt, Effect of relative humidity and air temperature on the results obtained from low-cost gas sensors for ambient air quality measurements, Sensor 20 (18) (2020) 5175, https://doi.org/10.3390/s20185175.
[30] J.D. Gutiérrez-Cano, P. Plaza-González, A.J. Canós, B. García-Baños, J.M. Catalá-Civera, F.L. Peñaranda-Foix, A new stand-alone microwave instrument for measuring the complex permittivity of materials at microwave frequencies, IEEE Trans. Instrum. Meas. 69 (6) (2019) 3595–3605. https://www.doi.org/10.1109/TIM.2019.2941038.
[31] R. Pérez-Campos, J. Fayos-Fernández, J. Monzó-Cabrera, Permittivity measurements for roasted ground coffee versus temperature, bulk density, and moisture content, JMPEE 57 (2) (2023) 102–116. https://www.doi.org/10.1080/08327823.2023.2206666.
[32] P. Song, X. Wu, S. Wang, Effect of styrene butadiene rubber on the light pyrolysis of the natural rubber, Polym. Degrad. Stab. 147 (2018) 168–176, https://doi.org/10.1016/j.polymdegradstab.2017.12.006.
[33] J. Croquesel, C. Meunier, C. Petit, F. Valdivieso, S. Pillon, A.C. Robisson, F. Lemont, Design of an instrumented microwave multimode cavity for sintering of nuclear ceramics, Mater. Des. 204 (2021), 109638, https://doi.org/10.1016/j.matdes.2021.109638.
[34] J. Shao, J. Zarling, Thermal conductivity of recycled tire rubber to be used as insulating fill beneath roadways, DOT&PF. No. INE/TRC 94.12, 1995. <https://trid.trb.org/view/643045>.
[35] C. Scarborough, Tyre temperature sensors, high power media, 2014. <https://www.highpowermedia.com/Archive/tyre-temperature-sensors> (Accessed on 21 December 2022).

[36] O. Xu, M. Li, D. Hou, Y. Tian, Z. Wang, X. Wang, Engineering and rheological properties of asphalt binders modified with microwave preprocessed GTR, Constr. Build. Mater. 256 (2020), 119440, https://doi.org/10.1016/j.conbuildmat.2020.119440.

[37] C. Nah, J.H. Park, C.T. Cho, Y.W. Chang, S. Kaang, Specific heats of rubber compounds, J. Appl. Polym. Sci. 72 (12) (1999) 1513–1522, https://doi.org/10.1002/(SICI)1097-4628(19990620)72:12<1513::AID-APP2>3.0.CO;2-I.

[38] A. Zanchet, F.D.B. de Sousa, Elastomeric composites containing SBR industrial scraps devulcanized by microwaves: raw material, not a trash, Recycling 5 (1) (2020) 3, https://doi.org/10.3390/recycling5010003.

[39] M.J. Fernández-Berridi, N. González, A. Mugica, C. Bernicot, Pyrolysis-FTIR and TGA techniques as tools in the characterization of blends of natural rubber and SBR, Thermochim. Acta 444 (1) (2006) 65–70, https://doi.org/10.1016/j.tca.2006.02.027.

[40] M. Vahdatbin, M. Jamshidi, Using chemical agent in microwave assisted devulcanization of NR/SBR blends: an effective recycling method, Resour. Conserv. Recycl. 179 (2022), 106045, https://doi.org/10.1016/j.resconrec.2021.106045.